VERSITA

Acta Geophysica
vol. 57, no. 4, pp. 923-949
DOI: 10.2478/s11600-009-0025-6

Katabatic Flow Induced by a Cross-Slope Band of Surface Cooling

Bryan A. BURKHOLDER, Alan SHAPIRO, and Evgeni FEDOROVICH

School of Meteorology, University of Oklahoma, Norman, OK, USA
e-mails: Bryan.A.Burkholder-1@ou.edu, ashapiro@ou.edu, fedorovich@ou.edu

Abstract

This paper investigates the behavior of katabatic flow induced by an idealized, thermally inhomogeneous surface; a strip of surface cooling that has a finite width in the along-slope direction and is infinitely long in the cross-slope direction. Numerical simulations using the Boussinesq equations of motion and the thermodynamic energy equation are performed for various slope angles and strip lengths. The underlying dynamical processes in the katabatic jet and the near environment are explored by considering the along-slope momentum balance after a steady state has been achieved.

The inhomogeneous nature of the surface forcing also induces a response in the environment that extends very far away from the sloped surface. Nearly horizontal jets close to the vertical heights of both sides of the cold strip are observed in the environment. A horizontal vorticity analysis is performed on these horizontal jets to ascertain their dynamical structure.

Key words: katabatic flow, thermally inhomogeneous surface, stratified flow, horizontal jets, slope flow.

1. INTRODUCTION

Thermally induced flow along sloping terrain within a stably-stratified environment can be found over a broad range of scales: from synoptic-scale motions in Antarctica to sub-mesoscale valley drainage flows. While analytical

solutions for thermally driven slope flows in stratified environments have been known for decades (Prandtl 1942, Defant 1949), these solutions are limited to homogeneous surface conditions. However, natural terrain is seldom homogeneous and can have spatially varying properties such as roughness, snow cover, vegetation coverage and/or type, soil type, and moisture content. In addition, external factors such as differential cloud cover or partial shading can also lead to spatially heterogeneous thermal properties of the sloping surface.

The purpose of this paper is to gain insight into the effects of surface inhomogeneity on katabatic flow in a stably-stratified environment by considering a simple inhomogeneous flow scenario associated with an isolated cross-slope band of surface cooling. This idealized forcing is roughly corresponds to surface conditions found near the ablation zone of various glaciers (Martin 1975, Van den Broeke *et al.* 1994, Oerlemans *et al.* 1999, Ágústsson *et al.* 2007), over small snow patches in sloping terrain (Ohata and Higuchi 1979), as well as conditions typical of nocturnal drainage flows along valley walls (Yoshino 1984, Mori and Kobayashi 1996, Gohm *et al* 2009). While the surface representation in our idealized model is not nearly as complex as what may be observed in nature, it provides a conceptually simple framework to observe the effects of local inhomogeneity.

Prandtl (1942) obtained exact analytical solutions to the Boussinesq equations of motion and the thermodynamic energy equation for the steady flow of a viscous fluid down a uniformly cooled surface within a stably-stratified environment. In the Prandtl model, the along-slope momentum equation describes a balance between the along-slope buoyancy and slope-normal diffusion of velocity. The balance in the thermodynamic energy equation is between the along-slope advection of environmental buoyancy (from the ambient stratification) and the diffusion of the buoyancy. These balances lead to a wind profile normal to the surface that is characterized by a low-level jet with weak return flow above the jet. The corresponding buoyancy perturbation decays rapidly with height, with a weak sign reversal in the flow aloft. This simple model compares qualitatively well with observations of katabatic flow when the mixing parameters are appropriately tuned (Tyson 1968, Papadopoulos *et al.* 1997, Oerlemans 1998) or prescribed as height-dependent variables (Grisogono and Oerlemans 2001). Similar profiles have also been observed in the analytical and numerical studies of natural convection flow along a heated vertical wall immersed in a stably-stratified fluid (Shapiro and Fedorovich 2004a, b).

While a homogeneous, one-dimensional model can sometimes provide a reasonable qualitative description of wind and temperature profiles for slope flows, predictions cannot be expected to compare well with observations of

flows over complex topography or flows dominated by spatially varying surface characteristics. In nature, the finite extent of the ice/snow ground coverage by glaciers or large snow patches on a sloped surface would violate the assumption of horizontal homogeneity made in the Prandtl model (Martin 1975, Nakamura 1976, Ohata and Higuchi 1979). The ambient air over a patch of ice/snow is cooled during the day, making the air negatively buoyant and causing it to accelerate downslope. The magnitude of the katabatic flow speed down the sloping surface is related to the fetch of the ice/snow ground cover that the air flows over (Ohata and Higuchi 1979, Ohata 1989). For nocturnal drainage flows found along a valley wall, the flow is not horizontally homogeneous due to the finite length of the sloping terrain. A katabatic jet is still observed along the valley wall, but the flow near the top of the valley ridge and the valley floor the exhibits drastically different behaviors compared to the Prandtl model (Yoshino 1984). Close to the top of the valley ridge, the downward accelerating flow induces subsidence, generating a region of higher temperatures compared to its immediate surroundings. This phenomenon is known as the **thermal belt**. It has been exploited for agricultural purposes for centuries (Kobayashi *et al*. 1994, Ueda *et al.* 2003). Meanwhile, the drainage flow forms a cold air lake at the bottom of the valley. As the cold air lake becomes deeper, the katabatic jet begins to flow over the top of the cold air lake, and also generates internal gravity waves (Mori and Kobayashi 1996). Dynamical effects close to the edges of the valley or ice/snow cover are not the only complicating factors introduced in geophysical katabatic flows. Physical obstructions, complex topography, cold patches, differential shading, and other types of surface irregularities can create additional characteristic scales on top of the larger characteristic scales of the background slope flow.

Mahrt (1982) performed a scale analysis on the downslope momentum equation for general classes of buoyancy driven slope flows to determine the dominant force balance under a variety of conditions. For the purposes of our study, the most relevant of these flows is a quasi-hydrostatic stationary flow with a negligible Coriolis force. The force balance in such a flow is determined by three parameters: the scaled flow depth ($\hat{H} = H/\Delta Z_s$, where H is a characteristic height of the flow and ΔZ_s is the total vertical height of the sloping surface), a Froude number ($F = U^2/g'H$, where U is a characteristic velocity of the flow, and g' is the reduced gravity), and a mixing/drag coefficient (C_D+k, where k is a general momentum exchange coefficient to account for entrainment). In terms of these parameters, the flows can be partitioned as an **equilibrium** flow

$$\hat{H} << 1\,, \quad F\hat{H} << 1\,, \quad F\left(C_D + k\right)/\sin\alpha = O(1)\,,$$

which corresponds to a balance between along-slope buoyancy and turbulent stress divergence, a **shooting** flow

$$\hat{H} << 1\,, \quad F\hat{H} \approx O(1)\,, \quad F\left(C_D + k\right)/\sin\alpha = O(1)\,,$$

conditioned by a balance between along-slope buoyancy, advection of momentum, and turbulent stress divergence, and an **advective-gravity** flow

$$\hat{H} << 1\,,\ F\hat{H} = O(1)\,, \quad F\left(C_D + k\right)/\sin\alpha << 1\,,$$

resulting from a balance between along-slope buoyancy and the advection of momentum. The solution obtained by Prandtl (1942), where the stress divergence and downslope component of buoyancy were of similar magnitudes, was classified by Mahrt as an equilibrium flow. However, in the case where surface inhomogeneities induce the flow, the along-slope advection of momentum may no longer be negligible, at least locally. Once this term becomes relevant to the problem [$F\hat{H} \approx O(1)$], the flow can no longer be classified as an equilibrium one and is classified, according to Mahrt (1982), as a shooting flow. This categorization of a shooting flow is fairly general and is typically applied to shallow flows exhibiting Froude numbers much larger than unity, such as the flows considered by Ball (1956), Ellison and Turner (1959), Tang (1976), and Manins and Sawford (1979). Geometrical properties of the surface irregularity that induced the shooting flow also become important when indentifying the flow type near the surface, as well as the environmental response. Mahrt considered analytic solutions for different idealized flow types using his scale analysis. One of these solutions corresponds to a shooting flow induced by a step-function of buoyancy near the surface. Mahrt found a solution for this flow by assuming a constant flow depth and a balance between the along-slope advection of momentum, turbulent transport, and along-slope buoyancy. This simple solution was found to approach the solution for an equilibrium flow after a certain length scale (proportional to the depth of the flow and the stress divergence) had been exceeded. To arrive at this solution, Mahrt assumed the depth of the thermal boundary layer to be known, and the velocity and buoyancy fields to vanish at the upper edge of the thermal boundary layer with velocity also vanishing at the slope surface. This simple solution did not reproduce the effects of the inhomogeneous buoyancy forcing on the environment and did not account for feedbacks between the environmental flow and the boundary layer.

The surface heterogeneity considered in our study is represented by an isolated cross-slope band (strip) of surface cooling. The band has finite

width in the along-slope direction, but is infinite in the cross-slope direction. This band is the only thermal (buoyancy) forcing on an assumed infinite planar slope and as such, is isolated. Egger (1981) and Kondo (1984) also investigated an isolated surface heterogeneity of a similar type and under analogous conditions, but with surface heating instead of cooling. Their analyses involved linearized Boussinesq equations of motion and thermodynamic energy about a motionless state. In our study, we numerically solve the full Boussinesq equations of motion and thermodynamic energy, thus retaining the non-linear terms neglected in the studies of Egger and Kondo. However, in both our case and Egger's case, the lateral boundary conditions are taken to be periodic, even though realistic slopes have finite length. Egger explicitly assumed that the region encompassed by the environmental response is contained within his solution domain, so that the adverse (unphysical) effects of periodic boundary conditions could be minimized. In our numerical setup, we attempt to satisfy a similar condition of an approximately isolated disturbance by placing our cold strip between large buffer zones of zero thermal forcing. In Egger's study, a thermally direct circulation, characterized by nearly horizontal flow in the environment and a Prandtl-like jet over the interior of the band of surface heating, developed and attained a steady state. The katabatic flow case in our study should exhibit a qualitatively similar structure to that solution. The expected flow structure following the analysis of Egger (1981), but for the katabatic flow case, is sketched in Fig. 1. In Egger's case with a 30° slope, a steady-state anabatic flow formed quickly over the heated patch, but the associated thermal circulation in the environment needed a much longer time to develop and reach a quasi-steady state. The steady-state flow far from the slope surface was characterized by horizontal outflow and inflow jets at nearly the same elevations as the edges of the heated strip. Egger found that the formation of these jets was primarily due to diabatically generated pressure differences that were located on either side of the heated strip. Flow between the environmental jets was relatively weak. Egger also found rough agreement between the Prandtl model and his results over the band of surface heating, but only for interior areas far from the strip edges. In this two-dimensional flow scenario, the one-dimensional Prandtl solution tended to underestimate the return flow aloft over the band of surface heating and, not surprisingly, the model was largely inappropriate in regions near the edges of the heated strip.

The studies of Egger (1981) and Kondo (1984) suggested the general structure of the environmental response to a cross-slope band of surface heating for a wide range of slope angles. While Egger applied his analysis to flows along a horizontal surface and relatively steep sloping surfaces (angles of 30° and 60°), Kondo focused on flows along shallow slopes. For very

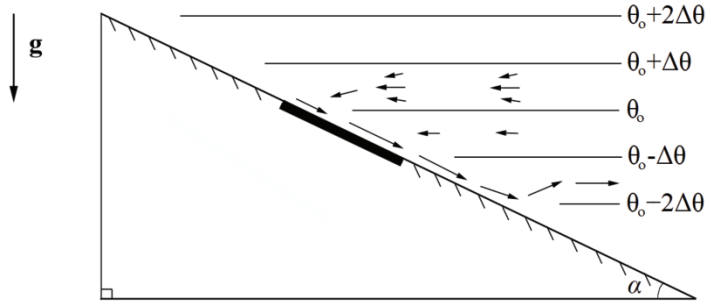

Fig. 1. Schematic of environmental flow induced by an imposed surface cold strip. Thin solid lines depict the environmental isentropes. The cross-slope band of surface cooling (cold strip) is shown as the thick black line on the slope surface. A jet is directed toward the upslope edge of the cold strip along environmental isentropes. An analogous jet, which is directed into the environment, develops at some distance down slope from the lower edge of the strip. A Prandtl-like jet is located directly above the band.

small slope angles, Kondo found that the flow behaved more like a heat island located on a horizontal surface rather than an anabatic slope flow. For these very small slope angles, a two-cell circulation similar to the flow pattern over a heat island on a flat surface was observed, but the circulation was slightly asymmetric about the center of the heated band. As the slope angle was increased, the flow over the band became more jet-like. This, on top of the effects of the environmental stratification, enhanced the asymmetry of the circulation, with one cell becoming dominant. At some critical slope angle, the two-cell circulation was completely replaced by a one-cell circulation (similar to the flow illustrated in Fig. 1). This critical angle was achieved once a vertical length scale, defined as the projection of one half of the length of the heated strip onto the true vertical direction, became equal to the height of a boundary layer over a horizontal heat island for the same magnitude of surface heating. This critical angle was also shown to be the angle at which the jet-like flow over the heated portion of the slope was exhibiting structure similar to the idealized Prandtl solution. It is not clear why, according to Kondo (1984), the depth of the thermal boundary layer for the flat-surface heat island should be comparable to half-width of a sufficiently long heated strip on a slope.

The idea that a Prandtl-like jet is observed after some critical length scale also follows from Mahrt's (1982) simple solution for a shooting flow. Mahrt assumed that the stagnancy of the environmental flow is a precondition for this solution, even though the results of Egger (1981) and Kondo (1984) suggest that this may not be a generally valid assumption. However, Mahrt

did include the advection of momentum in his solution, which is an effect that neither Egger nor Kondo accounted for. In anabatic flows investigated by Kondo and Egger, the non-linear advection terms may be dynamically significant near the surface, especially near the edges of the strip.

In the present study, we explore the characteristics of response of the stably stratified environmental flow to katabatic flow induced by surface cooling of finite width in the cross-slope direction (Fig. 1). While the orientation and geometry of the surface discontinuity are simplistic, the results may serve as a conceptual building block for understanding more complicated inhomogeneous katabatic flows. Using this particular surface buoyancy forcing, the Boussinesq equations of motion and thermodynamic energy are solved numerically. Past studies (Egger 1981, Mahrt 1982, Kondo 1984) suggest that two or more dynamical regimes may coexist in the flow with the surface forcing that considered herein. The *op.cit.* studies also suggest that the flow structure will depend significantly upon the slope inclination.

By using numerical simulation output, we will directly calculate the dominant force balances of along-slope momentum found in the katabatic jet near the surface under a variety of slope angles and strip widths. Additionally, we will determine the physical processes responsible for the existence of the horizontal jets in the environment by performing a steady-state horizontal vorticity analysis. Our aim is to provide a clear understanding of the underlying physics for an idealized inhomogeneous katabatic flow and its effect on the surrounding environment.

2. GOVERNING EQUATIONS

We consider the Boussinesq equations of two-dimensional motion and thermodynamic energy. As in Prandtl (1942), Egger (1981), Kondo (1984), and Shapiro and Fedorovich (2007), we work in a rotated Cartesian coordinate system where x and z are the along-slope and slope-normal coordinates, respectively (Fig. 2). In these coordinates, the governing slope flow equations are:

$$\frac{\partial u}{\partial t}+u\frac{\partial u}{\partial x}+w\frac{\partial u}{\partial z}=-\frac{\partial \pi}{\partial x}-b\sin\alpha+\nu\left(\frac{\partial^2 u}{\partial x^2}+\frac{\partial^2 u}{\partial z^2}\right), \tag{1}$$

$$\frac{\partial w}{\partial t}+u\frac{\partial w}{\partial x}+w\frac{\partial w}{\partial z}=-\frac{\partial \pi}{\partial z}+b\cos\alpha+\nu\left(\frac{\partial^2 w}{\partial x^2}+\frac{\partial^2 w}{\partial z^2}\right), \tag{2}$$

$$\frac{\partial b}{\partial t}+u\frac{\partial b}{\partial x}+w\frac{\partial b}{\partial z}=-N^2\left(-u\sin\alpha+w\cos\alpha\right)+\kappa\left(\frac{\partial^2 b}{\partial x^2}+\frac{\partial^2 b}{\partial z^2}\right), \tag{3}$$

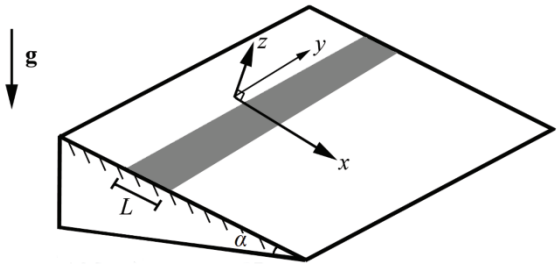

Fig. 2. Geometry of the imposed surface cooling and the coordinate system: x increases in the downslope direction, and z increases in the slope-normal direction. The strip is infinite in the cross-slope y-direction and has a length L in the along-slope direction.

$$\frac{\partial u}{\partial x}+\frac{\partial w}{\partial z}=0. \tag{4}$$

Here u and w are the along-slope and slope-normal components of velocity, respectively, ν is the kinematic viscosity, κ is the thermal diffusivity, π is a normalized pressure perturbation, α is the slope angle, and N is the environmental Brunt-Väisälä frequency. Buoyancy b is introduced as

$$b = g\frac{\theta-\theta_\infty}{\theta_r}, \tag{5}$$

where θ is the potential temperature, θ_∞ is the height-dependent environmental potential temperature, and θ_r is a constant reference potential temperature. Following Prandtl (1942) and Egger (1981), we consider an environmental potential temperature that increases linearly with height, which results in a constant Brunt-Väisälä frequency.

On the top boundary of the computational domain, zero normal gradient conditions are imposed on all prognostic variables, while at the bottom of the domain a no-slip condition is imposed on the along-slope and cross-slope velocity components, and the impermeability condition is imposed on the slope-normal velocity component.

The lower boundary condition for buoyancy is specified as

$$b(0)=b_s \quad \text{for } x\in[0,L) \quad \text{and} \quad \left.\frac{\partial b}{\partial z}\right|_{z=0}=0 \quad \text{for } x\in(-\infty,0)\cup[L,\infty), \tag{6}$$

where L is the length of the band of surface cooling, and b_s is the surface buoyancy imposed over this band.

The physical mechanism that causes the cooling is not the focus of our analysis. What is important for our study is that this differential cooling ex-

ists. The cooling could be induced by a variety of physical phenomena such as ice/snow cover, radiational forcing, or partial shading. In the model, the area of surface cooling is surrounded by large buffer zones to isolate the surface temperature disturbance and its environmental response. The surface boundary condition for buoyancy in the buffer zone is taken to be zero gradient so that the katabatic flow cools the surface as it propagates downslope. We have also performed simulations using a surface buoyancy of zero in the buffer zone, but these showed only minor qualitative differences from the simulations with zero-gradient buffer zones and will not be shown. Our initial field is taken to be a motionless state: $[u, w, \pi, b] = 0$ everywhere in the domain. In this respect, we can observe the environmental response to an isolated strip of surface cooling without any external complicating factors. At the beginning of the simulation, the buoyancy forcing described in (6) is suddenly imposed, and this induces the subsequent katabatic flow.

If we were to consider the buoyancy boundary conditions at the slope surface to be homogeneous rather than inhomogeneous, then in a steady state we would obtain the flow given by Prandtl (1942)

$$U = -b_s \left(\frac{1}{N^2 \,\mathrm{Pr}} \right)^{1/2} \mathrm{e}^{-\frac{z}{l}} \sin \frac{z}{l}, \tag{7}$$

$$b = b_s \, \mathrm{e}^{-\frac{z}{l}} \cos \frac{z}{l}, \tag{8}$$

$$l = \left(\frac{2\nu}{N \sin \alpha} \right)^{1/2} \mathrm{Pr}^{-1/4}, \tag{9}$$

where $\mathrm{Pr} = \nu/\kappa$ is the Prandtl number. This solution is anticipated to be the limiting solution for (1) – (4), (6) as $L \to \infty$. Even if L is finite, but sufficiently large, one may expect the vertical profiles sampled above the interior portions of the strip and far away from its edges, to be similar to the profiles given by (7) – (9). However, in view of the environmental response to the finite band of surface buoyancy forcing (horizontal inflow and outflow jets, as well as the possibility of gravity waves), it is not obvious how large L should be before the flow becomes Prandtl-like.

We solve (1) – (4), (6) numerically in a fashion similar to that of Shapiro and Fedorovich (2008). The equations are discretized onto staggered grids of various sizes, depending upon the simulated flow configuration (Table 1). Spatial derivatives are second order in space, and the integration in time is performed by a leapfrog scheme with a weak Asselin filter to prevent step decoupling. Pressure is diagnosed at every time step by solving a Poisson equation. To simulate two-dimensional flows, we use a three-dimensional

numerical code with the minimum number of grid points in the cross-slope (y) direction required to satisfy periodic boundary conditions in the cross-slope direction.

Since the lateral boundaries are periodic, the simulation of a seemingly isolated cold strip requires the numerical domain to be much larger than the length of the cold strip, so that the effects of periodicity are minimized. Flow due to a single cold strip in a finite domain with periodic boundaries is equivalent to flow due to an infinite number of separated cold strips in an infinite domain. The flows induced by each of the individual cold strips can interact with each other, for example, through pressure disturbances, if the separation between the cold strips is not large enough. If a strip is not sufficiently far from the computational boundaries, these effects can have a significant impact on the solution inside of the computational domain. To mitigate this problem, we impose a zero normal buoyancy gradient, eq. (6), at the bottom boundary in very large buffer zones that extend from the edges of the cold strip to the lateral boundaries. Likewise, Egger (1981) found that the environmental response to a thermal forcing of finite width on a slope can induce flow far away from the surface. This suggests that we must implement a computational domain that is as long (in x) and tall (in z) to contain the environmental response well within the bounds of the domain. However, we must also use grids with spacings that are fine enough to resolve the shallow Prandtl-like jet near the surface that we expect to form (Mahrt 1982). With these conditions in mind, and given our computational resources, we limited domain sizes and grid spacings in our simulations to those listed in Table 1.

Applying the Π theorem (Kundu and Cohen 2004) to (1) – (4) subject to the buoyancy boundary condition (6), we can establish the number of independent non-dimensional variables of the problem. Considering all of the variables in our problem (α, b_s, ν, κ, L, N, π, u, w, b, x, z) and taking into account their individual dimensions, we can form a set of six dimensionless variables

$$B = \frac{b}{|b_s|},\ U = \frac{uN}{|b_s|},\ W = \frac{wN}{|b_s|},\ \pi_n = \frac{\pi N^2}{b_s^{\,2}},\ X = x\sqrt{\frac{N}{\nu}},\ Z = z\sqrt{\frac{N}{\nu}}, \tag{10}$$

along with four independent non-dimensional Π groups

$$\Pi_1 = \alpha,\quad \Pi_2 = L\sqrt{\frac{N}{\nu}},\quad \Pi_3 = \frac{b_s}{\sqrt{\nu N^3}},\quad \Pi_4 = \frac{\nu}{\kappa}. \tag{11}$$

This set of four non-dimensional Π groups allows the relations between parameters of our problem to be expressed in a suitable form, even though it is not unique. The set (11) is convenient to interpret, since each Π group is

Table 1

Summary of numerical experiments undertaken. Grid dimensions are given by the along-slope, cross-slope, and slope-normal domain lengths, respectively. The name of each simulation is arranged in the following format: Case (α, L, $|b_s|$) with b_s in ms^{-2}.

Simulation	L [m]	Grid dimensions [m]	Grid spacing [m]	α [°]
Case (0°, 64, 0.1)	64	8192×8×1000	2	0
Case (0°, 1024, 0.1)	1024	16384×8×2000	2	0
Case (5°, 2048, 0.1)	2048	16384×4×500	1	5
Case (20°, 64, 0.1)	64	4096×8×1000	2	20
Case (20°, 2048, 0.1)	2048	16384×8×2000	2	20
Case (20°, 2048, 0.03)	2048	16384×8×2000	2	20
Case (90°, 1024, 0.1)	1024	4096×8×4000	2	90

characterized by a unique physical parameter (angle of inclination, length of the cold strip, and the imposed surface buoyancy). We adopt a naming convention for each simulation based on these physical parameters in the form Case (α, L, $|b_s|$) with b_s in ms^{-2}. Using (11), we can limit the number of simulations needed to explore the behavior of the solution.

In the simulations described hereafter, the Prandtl number is set to unity, thus limiting the number of independent parameters of our problem to three. Additionally, we set $N = 0.01$ s^{-1} and $\nu = 1$ m^{2}s^{-1}, which may be considered as typical values for general atmospheric conditions.

3. RESULTS

3.1 General flow characteristics

First, we consider the case of a band of surface cooling on a horizontal surface ($\alpha = 0°$). In this case, the environmental potential temperature gradient is perpendicular to the surface. Figure 3 shows a vertical cross-section of streamlines in the Case (0°, 1024, 0.1) flow after a quasi-steady state has been achieved. Negatively buoyant fluid flows away from the cold strip as a density current near the surface. Directly over the cold strip, fluid subsides toward the surface. With the stable stratification of the environment acting to suppress vertical motion, fluid is preferentially drawn along the horizontal environmental isentropes (Vergeiner and Dreiseitl 1987, Shapiro and Fedorovich 2007, 2008).

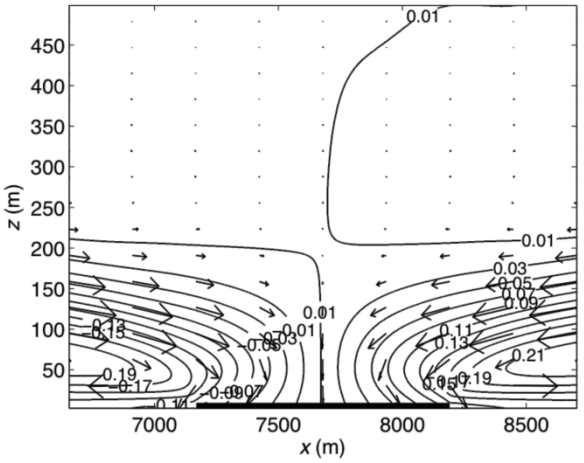

Fig. 3. Streamlines and wind vectors (arrows) for Case (0°, 1024, 0.1) about two hours (7680 seconds) after the surface cooling was imposed. The thick black line indicates the cold strip. For illustrative purposes, only a portion of the computational domain is presented. Vectors are plotted every 128 points in the *x*-direction and every 16 points in *z*-direction.

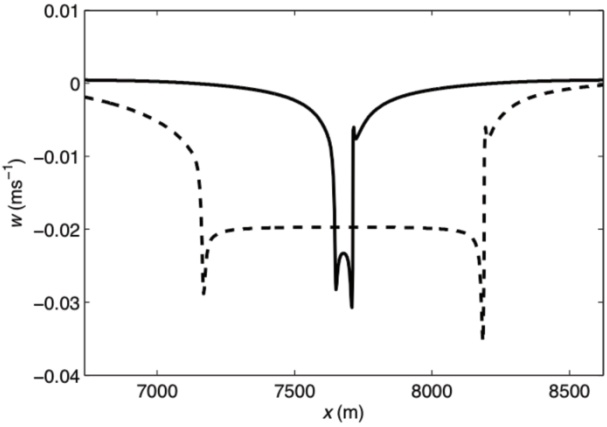

Fig. 4. Comparison of the slope-normal velocities at the 4-m level above the slope for Case (0°, 64, 0.1) (solid curve) and Case (0°, 1024, 0.1) (dashed curve). Lines are centered over the strips.

Figure 4 illustrates vertical fluid motion for two flow cases with $\alpha = 0°$, same values of buoyancy forcing, environmental stratification, and kinematic viscosity, but with different cold strip lengths. Each case displays downward motion over the strip interior, with the largest magnitudes of vertical motion very close to the edges of the cold strip. Due to the inexact placement of the cold strip relative to the domain boundaries, slight asymmetries are

present in the velocity distributions. Two nearly symmetric thermal circulations are clearly observed in Fig. 3, which are analogous to observed circulation features for $\alpha = 0°$ from Egger (1981) and Kondo (1984), taken with a negative sign, and to the flows pattern around a heated band observed in water tank experiments of Kimura (1975).

As the slope angle is increased from 0°, the flow behavior drastically changes. This can clearly be seen by comparing the steady state solution of Case (5°, 2048, 0.1) in Fig. 5 with the horizontal surface case shown in Fig. 3. Negatively buoyant fluid generated by the band of surface cooling flows down the slope until it is no longer negatively buoyant. The same behavior has been observed in nocturnal drainage flows by Yoshino (1984) and Mori and Kobayashi (1996), who found that negatively buoyant air flows down the valley slope until it reaches the top of the cold air lake. On the upslope edge of the cold strip, nearly horizontal flow from the environment to-

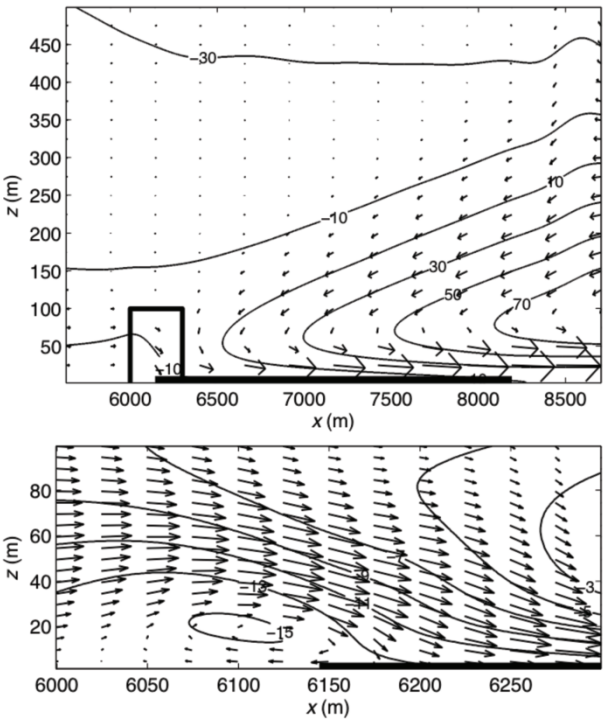

Fig. 5. Streamlines and velocity vectors for Case (5°, 2048, 0.1). The region near the upslope edge of the strip (bold rectangle in the top panel) is expanded in the bottom panel. Plots are shown 3120 s after the cold strip was imposed at the surface. The thick solid strip at the bottom indicates the position of the imposed surface cooling. In the top (bottom) panel, vectors are plotted every 256 (25) points in the x-direction and every 25 (5) points in the z-direction.

ward the surface is observed, and a small rotor forms directly upslope from the cool band. The horizontal environmental flow is a direct consequence of the acceleration down slope due to the abrupt change in surface thermal forcing, and is similar to the flow observed by Shapiro and Fedorovich (2007) for the case of gradual (linear) downslope changes in surface buoyancy. Upslope from the cold strip and away from the surface (with x in the range from 6000 to 6100 m and z about 60 m), nearly horizontal along-isentrope flow is induced in a similar manner. However, this latter flow is much weaker due to the effects of the ambient stratification.

The weak reverse flow directly upslope of the cold strip (at x from 6075 to 6160 m and $z = 10$ m) is attributable to the pressure gradient force, which will be discussed later while analyzing force balances in Section 3.3. Kondo (1984) identified the critical angle that should be reached before this upslope rotor completely disappears. Using the solution from his linear analysis, Kondo found that when the vertical projection of half-strip width ($L/2$) exceeded a depth scale of the thermal boundary layer over an identically heated strip on a horizontal surface, the velocity profile approached the Prandtl (1942) solution. This observed structural disparity between density current flows over horizontal surface and katabatic flows over sloping surface is intriguing, as it manifests principally different flow regimes in terms of dynamical balances (see Section 3.3).

The environmental flow in the numerical simulation for a larger slope angle, Case (20°, 2048, 0.03; illustrated in the top panel Fig. 6), again reveals flow structural features similar to the ones observed in the studies of Egger (1981) and Kondo (1984). Fluid moving toward the cold strip from the buffer zone and across the upslope edge of the cold strip experiences a drastic decrease in buoyancy (buoyancy is negative and increases in magnitude). This induces accelerating flow down the slope, and pulls in fluid nearly horizontally from the environment, as in the case of gradually-varying surface buoyancy (Shapiro and Fedorovich 2007). An analogous gentle horizontal environmental motion toward the slope was found in slope wind solutions of Egger (1981) and Kondo (1984). At the downslope side of the strip, at x from 8200 to 8500 m, negatively buoyant fluid travels some distance beyond the strip until it reaches its level of zero buoyancy. Beyond this level, the weakening katabatic jet enters the environment with features reminiscent of gravity currents and gravity waves. Due to the linearization adopted in the models of Egger (1981) and Kondo (1984), their solutions do not show the flow continuing along the slope beyond the thermally forced strip. In our simulation, the gravity waves generated by the overshoot of the level of zero buoyancy are transient in nature and propagate away from the surface. With moderate to steep slope angles (~20°) and strong buoyancy forcing (~0.1 ms^{-1}), standing waves are observed in the quasi-steady flow state at the level of zero

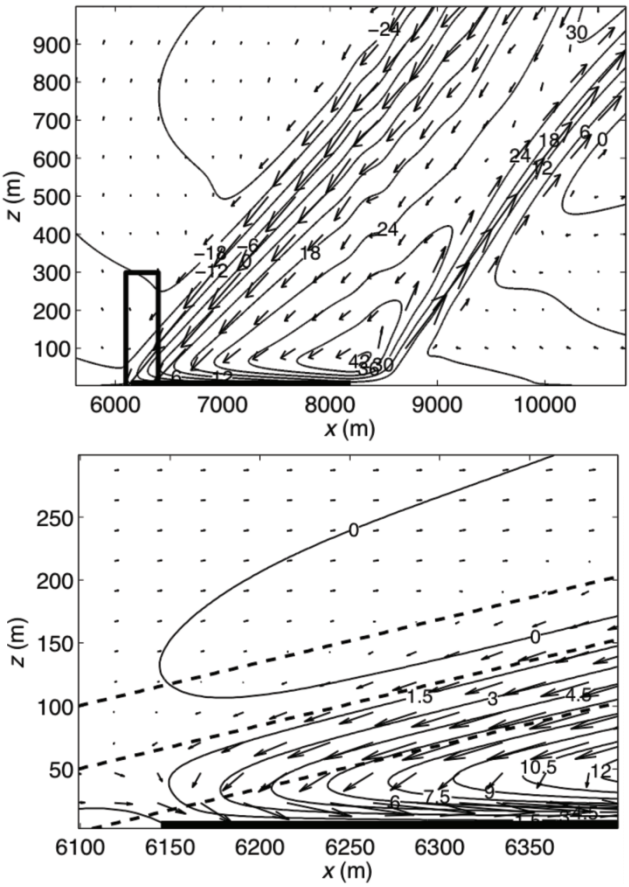

Fig. 6. Vertical cross-section of streamlines and velocity vectors in Case (20°, 2048, 0.03). The region near the upslope edge of the strip (bold rectangle in the top panel) is expanded in the bottom panel. The plots are taken 3501 s after the cold strip was imposed at the surface. Dashed lines in the bottom panel show true horizontal directions. Vectors in the top (bottom) panel are plotted every 128 (12) points in the x-direction and 50 (12) points in the z-direction.

buoyancy near the surface. However, in the case of an ultimately steep slope (vertical wall with $\alpha = 90°$), flow near the overshoot has been found to be perpetually unsteady. The observed horizontally propagating gravity waves travelling away from the surface eventually interact with the domain top boundary because of the domain orientation in the along-slope and slope-normal directions (see Fig. 2). Once this occurs, the reflected gravity waves slowly become more prominent in the solution until no other feature is distinguishable in the simulated flow fields. This numerical artifact is, unfortunately, an inevitable consequence of the employed numerical setup.

Accordingly, the numerical results shown in this study are for time periods long enough for a quasi-steady state to be achieved, but short enough for the reflected gravity waves not to contaminate the solution.

3.2 Environmental vorticity balance

In order to balance the mass flux associated with the flow acceleration near the upslope edge of the cold strip and the flow deceleration near the downslope edge (see Section 3.1), compensating slope-normal motions must exist. These motions appear as environmental inflow and outflow jets discussed in the previous section. Comparing Fig. 6 (top panel) with Fig. 7, we see that the largest values of the *y*-component of vorticity in the environmental flow are observed on the sides of the inflow and outflow jets. Evidently, the vorticity in these jets is primarily associated with strong flow shears across the jets. Velocity maxima within the jets are closely associated with zero values of vorticity.

To examine the processes that contribute to the vorticity balance in a steady state, we calculate individual terms in the horizontal vorticity equation

$$\frac{\partial \eta}{\partial t} + \mathbf{u} \cdot \nabla \eta = -\frac{\partial b}{\partial X} + \nu \nabla^2 \eta \,, \tag{12}$$

where η is the *y*-component of the vorticity, and $\mathbf{u}$ is the velocity vector. By analyzing inter-term balances in (12), we can identify the physical processes responsible for the creation and maintenance of the environmental inflow jet.

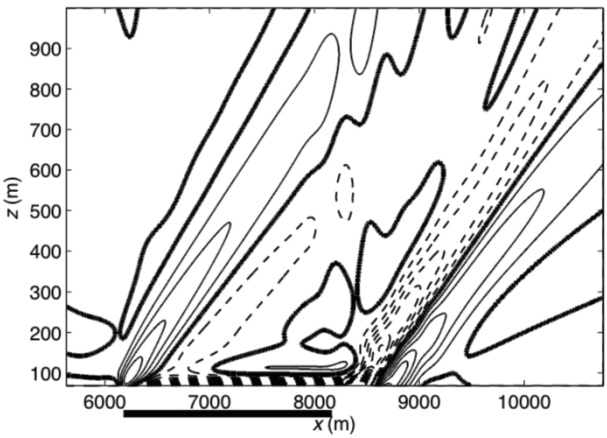

Fig. 7. A cross-sectional contour plot of η for the flow shown in Fig. 6. The lowest 50-m flow region is excluded to draw attention to the environmental flow. The position of the cold strip is indicated by the thick black line. Negative values of η are plotted as dashed lines, positive values are plotted as thin solid lines, and the zero vorticity contours are plotted as bold lines. The contour interval is 0.0005 s^{-1}.

The only possible source of vorticity in (12) is through baroclinic generation (represented by the first term on the right-hand side, where X denotes the direction along environmental isentropes and normal to y axis), since both diffusion and advection act on existing fields of vorticity.

Figure 8 shows values of vorticity tendency (vorticity production/destruction rate) along the slope at 50- and 200-m elevations above the slope for Case (20°, 2048, 0.03), which has already been considered in Figs. 6 and 7. These two levels are representative of the region where the environmental inflow jet interacts with the boundary layer (50 m) and the environmental region relatively far away from the boundary layer (200 m). Relating the tendency distributions from the two panels of Fig. 8 to the contoured vorticity field in Fig. 7, we see that vorticity (Fig. 7) tends to be of the same sign as the baroclinic generation term (Fig. 8).

For example, at $z = 200$ m, one of the positive vorticity regions in Fig. 7 can be found on the x range of 6300 m to 6650 m. This region is within the top half of the environmental inflow jet (Fig. 6, top), and is characterized by positive baroclinic vorticity generation (Fig. 8, bottom). Inflow jet streamlines

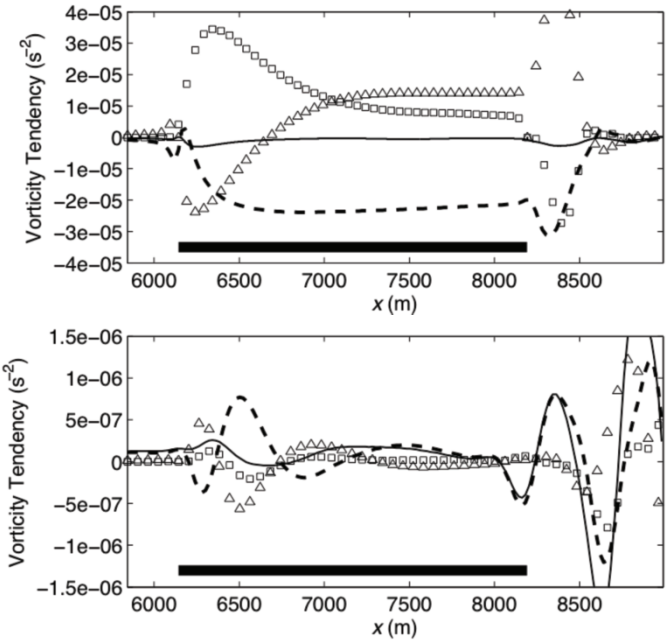

Fig. 8. Contributions to the tendency of horizontal vorticity at heights of 50 m (top) and 200 m (bottom) above the slope for the flow case illustrated in Figs. 6 and 7. Baroclinic generation (dashed), diffusion (triangles), and non-linear advection (squares) terms are calculated directly from the numerical output, while the non-stationary term (solid line) is assumed be the residual.

in the bottom panel of Fig. 6 exhibit slightly concave curvature toward the slope surface. Such local flow organization results in negative horizontal (in terms of X) buoyancy gradient, which leads to the positive vorticity generation above the jet. In the region above the inflow jet maximum, the streamline pattern is visually similar to the pattern obtained analytically by Yih (1980) for the two-dimensional inviscid flow into a mass sink. However, in our flow case, the baroclinic generation of vorticity in the environmental inflow jet is offset by diffusion (at $x = 6500$ m in Fig. 8, bottom panel). This suggests that despite the visual similarity, the environmental jets observed in our cases are not governed by the selective withdrawal mechanism discussed by Yih (1980). His solution assumes a balance between non-linear advection and baroclinic generation of vorticity, which may be the case for parameter ranges other than those considered in our study.

At 50-m elevation (Fig. 8, top), the vorticity balance is very different from the balance observed at 200-m height. This difference is due to the interaction between the environmental and boundary-layer flows at the lower elevation. The effect of the surface cooling is readily apparent from the large values of negative baroclinic vorticity generation. Assuming that Prandtl's solution is approximately valid at 50 m above the strip, one may expect that baroclinic generation and diffusion of vorticity would be the dominant balance terms in (12). However, unlike Prandtl's flow case, the non-linear terms at 50 m are significant even at distances far away from the upslope edge of the cold strip (at x between 7500 m and 8200 m). Referring to Figs. 6 and 7, we clearly observe vorticity advection into the boundary layer from the environment at 50 m; particularly from $x = 6250$ m to the downslope edge of the cold strip. Thus, the presence of vorticity advection associated with the environmental jet impacts the flow structure in the boundary layer above the strip.

The above result implies that for the parameter range considered, a linear analysis would be appropriate for the environmental flow, but not for flow regions where interactions between the environmental inflow jet and the katabatic jet take place. Hence, a linear analysis may provide a partial flow description for our case, but would not capture the entire scope of the dynamical balances.

More numerical experiments need to be conducted by varying the parameters in (11) to explore whether linear approximations are applicable for flows characterized by different parameter combinations. It may be the case that for larger L values, the non-linear terms would become negligibly small in regions far away from environmental inflow jet. Conversely, it is plausible that a balance similar to Yih (1980) may exist in the environment for smaller viscosities and/or larger buoyancy forcings.

3.3 Momentum balance in the katabatic jet

The question of how large L has to be to provide a katabatic jet with velocity and buoyancy profiles approximately similar to those of the Prandtl (1942) jet has not been sufficiently addressed in the literature. Figure 9 shows the slope-normal profiles of the along-slope velocity at different distances down slope from the upslope edge (0, 0.05, 0.1, 0.25, 0.5, and 0.75L) for Case (20°, 2048, 0.03) and Case (90°, 1024, 0.1). We will refer to the latter case as a wall case. As a reference, the Prandtl solution (7) for a homogeneous surface forcing (which corresponds to $L \to \infty$) is also displayed. In the wall case, the numerical solution shows excellent agreement with the Prandtl solution for a homogeneous surface after a fetch of cooling that is 75% of the strip length. Evidently, effects of the edges of the cold strip for this case are negligible. The wall case appears to be special, however, since the flow in Case (20°, 2048, 0.03) does not show very good of agreement with the homogeneous solution at any distance away from the upslope edge of the cold strip. It is possible that the cold strip was simply not broad enough (long enough in the slope direction) to produce a Prandtl flow regime. If that was the case, then the environmental inflow jet interactions with the boundary layer, pressure gradient forces opposing the downslope motion over the strip

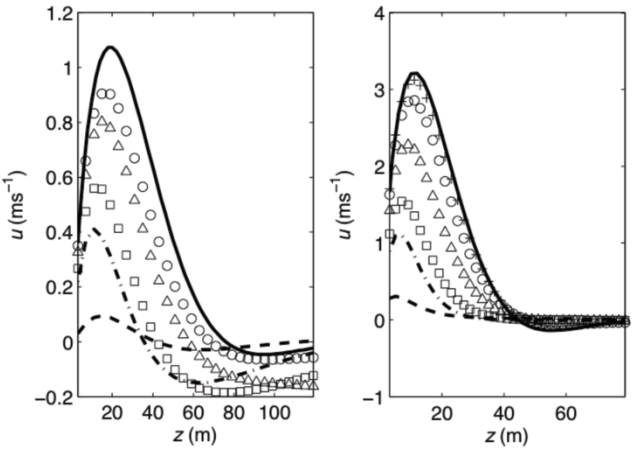

Fig. 9. Vertical profiles of the along-slope velocity component for Case (20°, 2048, 0.03) (left) and Case (90°, 1024, 0.1) (wall case, right) with different fetches of the surface cooling. Prandtl solution (solid) and the numerical results are plotted at different fractions of the strip length downslope from the upslope edge of the surface cooling: 0% (dashed), 5% (dash-dot), 10% (squares), 25% (triangles), 50% (circles), and 75% (crosses) of the length L of the surface cooling. In the left panel, the vertical profile at 0.75L away from the upslope edge of the surface cooling is not plotted because it is virtually identical to the profile at 0.5L, with both falling short of the Prandtl solution.

(generated by baroclinicity), or the effects of gentle slope-normal motion toward the slope over the entire cold strip (as shown in Fig. 4) could all impact the flow in the boundary layer and alter the shape of its buoyancy and velocity profiles.

To investigate downslope momentum balances over the cold strip (shown in Figs. 10 and 11), we evaluate individual terms in (1). This, in conjunction with our vorticity analysis, may provide suggestions regarding deviations of the observed profiles from the Prandtl solution in the simulated flow cases except for the wall case. The terms are calculated at the slope-normal height of the katabatic jet, since this is the height where the greatest along-slope acceleration occurs. The horizontal surface case (Fig. 10, upper plot) is characterized by a balance between the pressure gradient force and diffusion, which is typical for a flow similar to a density current. Flow in this

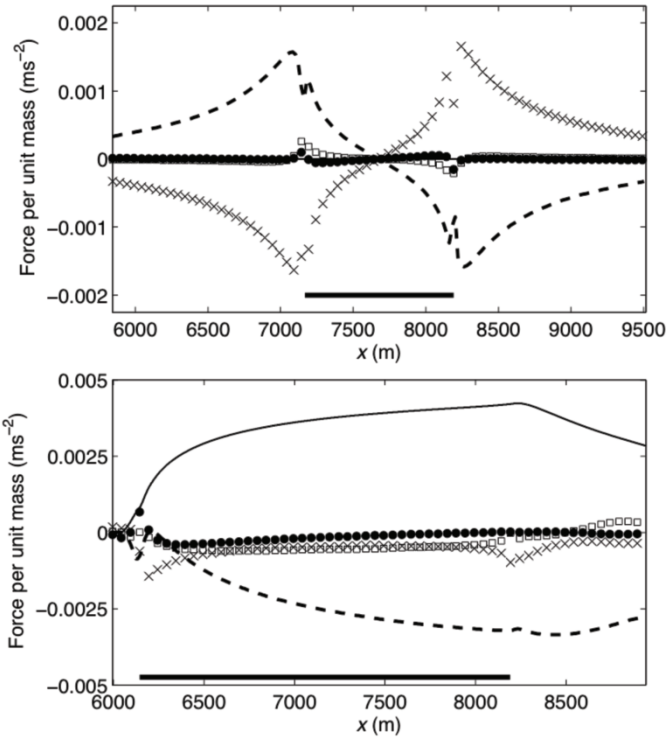

Fig 10. Along-slope momentum balances at the level of the boundary-layer jet for Case (0°, 1024, 0.1) (horizontal surface, top) and Case (5°, 2048, 0.1) (bottom). In each plot, a thick black line indicates the position of the cold strip. The momentum balance terms shown are along-slope buoyancy (solid line), diffusion (dashed), along-slope advection (squares), slope-normal advection (filled circles), and the pressure gradient (crosses).

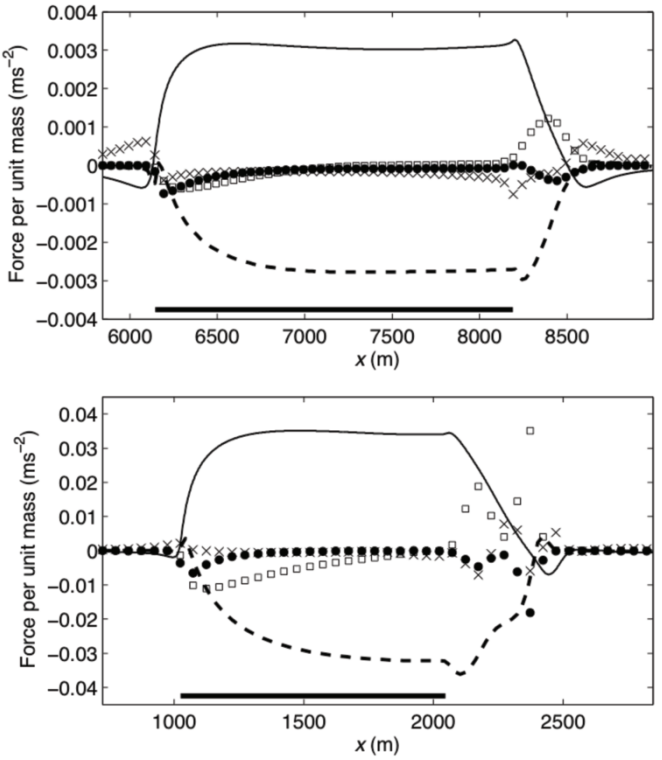

Fig. 11. Along-slope momentum balances for Case (20°, 2048, 0.03) (top) and Case (90°, 1024, 0.1) (wall case, bottom). For notation, see Fig. 10.

case is nearly symmetrical about a slope-normal axis positioned at the center of the cold strip. Likewise, the forcing terms in the momentum balance are nearly anti-symmetric about the same axis. For small slope angles (like in the bottom plot of Fig. 10), acceleration due to the along-slope buoyancy becomes a substantially more important component of the steady-state balance. Recall that in Case (5°, 2048, 0.1) a small rotor was observed near the upslope edge of the cold strip (see bottom plot of Fig. 5). The force balance associated with this rotor is shown in the bottom panel of Fig. 10 (for x in the range from 6075 m to 6160 m). The pressure gradient force acts to force fluid upslope, and is counter-balanced by along-slope buoyancy and slope-normal advection. Over a major portion of the cold strip, the flow is in a quasi-steady state with a primary balance between diffusion and along-slope buoyancy.

For large angles such as in Case (20°, 2048, 0.03), the momentum balance near the upslope edge of the cold strip (Fig. 11, top panel) is between the along-slope buoyancy, non-linear advection terms, and diffusion. This

balance corresponds to the type of flow that Mahrt (1982) classified as a shooting flow. The slope-normal advection of momentum provided by the environmental inflow jet affects the shape of the steady-state slope-normal profiles over the cold strip. This environmental inflow jet is relatively thick (see Fig. 6, top) and has a direct impact on the Prandtl-like jet near the surface. As the fluid moves down the slope over the cold strip, the momentum balance is established primarily between the buoyancy forcing and diffusion, which is analogous to the balance of momentum in the Prandtl model. However, despite the Prandtl-like form of momentum balance and the visual similarity of the simulated flow to the Prandtl flow (a pronounced downslope jet with a weak return flow), the numerical solution differs in some notable ways from the Prandtl solution (refer to Fig. 9, left panel). Recall that from the vorticity analysis (Section 3.2) that the non-linear terms were found to be significant directly above the boundary-layer jet (Fig. 8, top panel).

To help understand why we observe the same momentum balance as the Prandtl model but nevertheless obtain different velocity profiles, imagine an experiment where Prandtl solution is imposed at some level z above the surface. Applying homogeneous buoyancy forcing at the surface, one would eventually get a steady state flow regime corresponding exactly to the Prandtl solution. If we were to modify the condition at level z by changing velocity at this level to a homogeneous (in x) value other than given by the Prandtl solution at z, the resulting steady-state flow solution would differ from the Prandtl solution. However, since the boundary condition was homogeneous along the slope, the flow would still exhibit a momentum balance between diffusion and along-slope buoyancy. The above consideration suggests that the environmental inflow jet can influence the boundary layer jet by mimicking the effect of a boundary condition, leaving the Prandtl-like momentum balance in the boundary layer jet region intact.

In Case (90°, 1024, 0.1; Fig. 9, right), buoyancy and diffusion are offset by the non-linear advection terms at the upslope edge of the cold strip (for x in the range from 1000 m to 1500 m). As the distance from the upslope edge increases, the balance slowly becomes dominated by along-slope buoyancy and diffusion. One reason for the excellent agreement between the Prandtl solution and the flow over cold strip in this particular flow case is that the along-slope projection of the environmental jet is nearly zero in the along-wall flow. This minimizes the influence of the inflow jet on the boundary layer flow above the strip. Also, the projection of the horizontal (along-isentrope) jet onto the along-slope axis is at its minimum in the wall case. This means that at large distances downslope from the upslope edge of the cold strip, the environmental inflow jet will never be above the along-wall boundary-layer jet, ensuring that incoming jet and along-wall jet do not di-

rectly interact with each other. Downslope from the cold strip, the flow is essentially unsteady (characterized by spontaneous generation of gravity waves) and the momentum balance is rather inconsistent.

In each case shown in Figs. 10 and 11, the momentum balance exhibits effects caused by the interaction between the horizontal flow (jet) in the environment toward the slope and the boundary layer katabatic jet. The non-linear advection terms in the along-slope distributions show the along-slope range in which the environmental inflow jet affects the solution. As the slope angle increases, the width of the environmental jet projection onto the along-slope direction decreases. This can be seen in Fig. 10 as a decrease in the along-slope range of where the non-linear advection terms are close to zero over the strip. Thus, in order to achieve a Prandtl regime in shallow-slope ($< 10°$) flows, one would need to operate with much larger L values than the ones considered in this study.

4. CONCLUSIONS

Local katabatic flow induced by a strip-like thermal inhomogeneity across a sloping surface in a stably-stratified fluid has been numerically investigated. Simulated flow qualitatively corresponds to slope flow types considered in Egger (1981) and Kondo (1984). However in our flow case, some non-linear effects are apparent in the region of interaction between the environmental flow and katabatic jet near the surface. These non-linear effects are found to be most important near the edges of the cold strip considered.

The nearly horizontal jets observed in the environmental flow in a quasi-steady state have been analyzed in terms of the horizontal vorticity tendencies. It has been shown that flow in the jets is controlled through the balance between baroclinic vorticity generation and its destruction by diffusion. The advection of vorticity has been found relevant in regions where the environmental inflow jet impinges upon the top of the boundary layer flow. Neglecting the advection terms, as was done in the linear analyses of Egger (1981) and Kondo (1984), would be a fair approximation for most of the environmental flow, but not in the region where the environmental jet impacts on the boundary-layer katabatic jet. Non-linear effects have also been found to play a significant role in the momentum balance of the considered flow near the edges of the cold strip. Particular geometric characteristics of flow regions influenced by non-linear effects depend upon the slope angle, imposed surface buoyancy forcing, and strip width. If the strip is too narrow, the flow accelerates downslope over the entirety of the strip, and the non-linear and pressure gradient terms are important in the momentum balance over the whole strip width. Similarly, if the buoyancy forcing is large enough, a given strip may not be broad enough for flow to reach the balance found in the

equilibrium Prandtl (1942) flow. Likewise, for small slope angles (< 5°), the projection of the horizontal environmental inflow jet onto the along-slope direction becomes very large. This increases the fetch of surface cooling required to attain an equilibrium flow over the interior of the cold strip due to the interactions between the katabatic jet close to the surface and the nearly horizontal environmental inflow jet.

In most of reported experiments the strips have been relatively narrow, so the flow in the boundary layer over the cold strip for small angles has not exactly matched the solution given by Prandtl (1942). For the strip dimensions considered, the momentum balance in the along-slope direction is much more complex over the main portion of the strip than the balance in the Prandtl (1942) flow. The momentum balance observed in our simulations is similar to the balance attributed by Mahrt (1982) to a shooting slope flow. However in *op. cit.*, both linear and non-linear interactions between the environmental and the boundary layer flow have been neglected, while we found these processes to be quite important. With these interactions taken into account, a fetch larger than the one estimated by Mahrt is needed to approach the equilibrium solution. Similarly, Kondo (1984) did not consider the non-linear interaction between the environmental inflow jet and the Prandtl-like jet in his model of flow induced by a strip of surface heating. Thus, he also may have underestimated the length of the fetch needed to reach an equilibrium flow state. Interestingly, the non-linearity of the momentum balance aloft affects the flow near the surface and over the interior of the strip in such a way that the exact Prandtl solution is not attained over the entire strip, even though the along-slope momentum exhibits the same balance of along-slope buoyancy and diffusion near the surface. The flow profiles are generally rather similar to the Prandtl model counterparts, but the strength of the katabatic jet is attenuated by the interaction with the environmental flow above the katabatic jet. In contrast, the flow case with a very large angle, such as the flow along a vertical wall, has been found to match the Prandtl model almost exactly toward the downslope edge of the strip.

Our results suggest that simulations of more realistic (turbulent) flows over sloping terrain in a stably-stratified environment induced by patches of surface thermal heterogeneity should be conducted with sufficiently large domains to correctly account for the flow entering and exiting the boundary layer region along the slope. Even relatively small patches of thermal heterogeneity may induce horizontal flow along isentropes far away from the sloping surface. Knowing the general feature of the fluid response to the thermally irregular surface forcing might aid in interpreting cases of fully turbulent of flows over terrain with complex thermal properties.

Acknowledgements. The authors would like to thank the helpful comments received from the reviewers, which has led to the discovery of many relevant observational studies. This research was supported by the U.S. National Science Foundation under Grant ATM-0622745.

References

Ágústsson, H., J. Cuxart, A. Mira, and H. Ólafsson (2007), Observations and simulation of katabatic flows during a heatwave in Iceland, *Meteorol. Z.* **16**, 1, 99-110, DOI: 10.1127/0941-2948/2007/0189.

Ball, F.K. (1956), The theory of strong katabatic winds, *Aust. J. Phys*. **9**, 373-386.

Defant, F. (1949), Zür Theorie der Hangwinde, nebst Bemerkungen zür Theorie der Berg- und Talwinde, *Arch. Meteorol. Geophys. Bioklim*. *A* **1**, 3-4, 421-450, DOI: 10.1007/BF02247634.

Egger, J. (1981), On the linear two-dimensional theory of thermally induced slope winds, *Beitr. Phys. Atmos*. **54**, 465-481.

Ellison, T.H., and J.S. Turner (1959), Turbulent entrainment in stratified flows, *J. Fluid Mech*. **6**, 3, 423-448, DOI: 10.1017/S0022112059000738.

Gohm, A., F. Harnisch, J. Vergeiner, F. Obleitner, R. Schnitzhofer, A. Hansel, A. Fix, B. Neininger, S. Emeis, and K. Schäfer (2009), Air pollution transport in an Alpine valley: Results from airborne and ground-based observations, *Bound.-Layer Meteor*. **131**, 3, 441-463, DOI: 10.1007/s10546-009-9371-9.

Grisogono, B., and J. Oerlemans (2001), Katabatic flow: Analytic solution for gradually varying eddy diffusivities, *J. Atmos. Sci*. **58**, 21, 3349-3354, DOI: 10.1175/1520-0469(2001)058<3349:KFASFG>2.0.CO;2.

Kimura, R. (1975), Dynamics of steady convections over heat and cool islands, *J. Meteorol. Soc. Jpn*. **53**, 440-457.

Kobayashi, T., M. Mori, and K. Wakimizu (1994), An observational study of a thermal belt on hillsides, *J. Meteorol. Soc. Jpn*. **72**, 387-399.

Kondo, H. (1984), The difference of the slope wind between day and night, *J. Meteorol. Soc. Jpn*. **62**, 224-232.

Kundu, P.K., and I.M. Cohen (2004), *Fluid Mechanics*, 3rd ed., Elsevier Academic Press, San Diego.

Mahrt, L. (1982), Momentum balance of gravity flows, *J. Atmos. Sci*. **39**, 12, 2701-2711, DOI: 10.1175/1520-0469(1982)039<2701:MBOGF>2.0.CO;2.

Manins, P.C., and B.L. Sawford (1979), A model of katabatic winds, *J. Atmos. Sci*. **36**, 4, 619-630, DOI: 10.1175/1520-0469(1979)036<0619:AMOKW> 2.0.CO;2.

Martin, S. (1975), Wind regimes and heat exchange on Glacier Saint-Sorlin, *J. Glaciol*. **14**, 91-105.

Mori, M., and T. Kobayashi (1996), Interaction between observed nocturnal drainage winds and a cold air lake, *J. Meteorol. Soc. Jpn*. **74**, 247-258.

Nakamura, K. (1976), Nocturnal cold air drainage and distribution of air temperature on the gentle slope, *Geogr. Rev. Jpn*. **49**, 380-387.

Oerlemans, J. (1998), The atmospheric boundary layer over melting glaciers. **In:** A.A.M. Holtslag and P.G. Duynkerke (eds.), *Clear and Cloudy Boundary Layers*, Royal Netherlands Academy of Arts and Sciences, 129-153.

Oerlemans, J., H. Björnsson, M. Kuhn, F. Obleitner, F. Palsson, C.J.P.P. Smeets, H.F. Vugts, and J. De Wolde (1999), Glacio-meteorological investigations on Vatnajökull, Iceland, summer 1996: An overview, *Bound.-Layer Meteor*. **92**, 1, 3-24, DOI: 10.1023/A:1001856114941.

Ohata, T. (1989), Katabatic wind on melting snow and ice surfaces (II) application of a theoretical model, *J. Meteorol. Soc. Jpn*. **67**, 113-122.

Ohata, T., and K. Higuchi (1979), Gravity wind on a snow patch, *J. Meteorol. Soc. Jpn*. **57**, 254-263.

Papadopoulos, K.H., C.G. Helmis, A.T. Soilemes, J. Kalogiros, P.G. Papageorgas, and D.N. Asimakopoulos (1997), The structure of katabatic flows down a simple slope, *Quart. J. Roy. Meteor. Soc*. **123**, 542, 1581-1601, DOI: 10.1002/qj.49712354207.

Prandtl, L. (1942), *Führer durch die Strömungslehre*, Vieweg & Sohn, Braunschweig (in German).

Shapiro, A., and E. Fedorovich (2004a), Unsteady convectively driven flow along a vertical plate immersed in a stably stratified fluid, *J. Fluid Mech*. **498**, 333-352, DOI: 10.1017/S0022112003006803.

Shapiro, A., and E. Fedorovich (2004b), Prandtl number dependence of unsteady natural convection along a vertical plate in a stably stratified fluid, *Int. J. Heat and Mass Transfer* **47**, 22, 4911-4927, DOI: 10.1016/j.ijheatmasstransfer.2004.04.035.

Shapiro, A., and E. Fedorovich (2007), Katabatic flow along a differentially cooled sloping surface, *J. Fluid Mech*. **571**, 149-175, DOI: 10.1017/S0022112006003302.

Shapiro, A., and E. Fedorovich (2008), Coriolis effects in homogeneous and inhomogeneous katabatic flows, *Quart. J. Roy. Meteor. Soc*. **134**, 631, 353-370, DOI: 10.1002/qj.217.

Tang, W. (1976), Theoretical study of cross-valley wind circulation, *Arch. Meteor. Geophys. Bioklim*. *A* **25**, 1, 1-18, DOI: 10.1007/BF02245465.

Tyson, P.D. (1968), Velocity fluctuations in the mountain wind, *J. Atmos. Sci*. **25**, 3, 381-384, DOI: 10.1175/1520-0469(1968)025<0381:VFITMW>2.0.CO;2.

Ueda, H., M.E. Hori, and D. Nohara (2003), Observational study of the thermal belt on the slope of Mt. Tsukuba, *J. Meteorol. Soc. Jpn*. **81**, 5, 1283-1288, DOI: 10.2151/jmsj.81.1283.

Van den Broeke, M.R., P.G. Duynkerke, and J. Oerlemans (1994), The observed katabatic flow at the edge of the Greenland ice sheet during GIMEX-91, *Global Planet. Change* **9**, 1-2, 3-15, DOI: 10.1016/0921-8181(94)90003-5.

Vergeiner, I., and E. Dreiseitl (1987), Valley winds and slope winds – observations and elementary thoughts, *Meteorol. Atmos. Phys*. **36**, 267-286.

Yih, C. (1980), *Stratified Flows*, Academic Press, Inc., New York.

Yoshino, M.M. (1984), Thermal belt and cold air drainage on the mountain slope and cold air lake in the basin at quiet, clear night, *GeoJournal* **8**, 3, 235-250, DOI: 10.1007/BF00446473.

Received 13 February 2009
Accepted 8 July 2009